Commun. Comput. Phys.
doi: 10.4208/cicp.OA-2015-0008

Vol. **22**, No. 1, pp. 259-284
July 2017

# An Approach to Obtain the Correct Shock Speed for Euler Equations with Stiff Detonation

Bin Yu, Linying Li, Bin Zhang* and Jianhang Wang

*School of Aeronautics and Astronautics, Shanghai Jiao Tong University, Shanghai 200240, China.*

Communicated by Chi-Wang Shu

Received 6 November 2015; Accepted (in revised version) 16 November 2016

**Abstract.** Incorrect propagation speed of discontinuities may occur by straightforward application of standard dissipative schemes for problems that contain stiff source terms for underresolved grids even for time steps within the CFL condition. By examining the dissipative discretized counterpart of the Euler equations for a detonation problem that consists of a single reaction, detailed analysis on the spurious wave pattern is presented employing the fractional step method, which utilizes the Strang splitting. With the help of physical arguments, a threshold values method (TVM), which can be extended to more complicated stiff problems, is developed to eliminate the wrong shock speed phenomena. Several single reaction detonations as well as multi-species and multi-reaction detonation test cases with strong stiffness are examined to illustrate the performance of the TVM approach.

**AMS subject classifications**: 35Q31, 76L05

**Key words**: Detonation, spurious behavior, reactive Euler equations, threshold values method, stiffness.

## 1 Introduction

In simulating the reactive Euler equations with the homogeneous source terms, often applied in field of combustion and high speed chemical reacting, a well-known spurious numerical phenomenon which was observed firstly by Collela et al. [1], may occur if the equations are solved in the under-resolved conditions, namely the coarse grid, large time step or other combinations in conjunction with the type of spatial scheme and type of temporal discretization etc. [2–4]. By properly defining a model problem with a stiff source term, LeVeque and Yee [5] reveal that the typical spurious behavior which is the propagation error of the detonation wave, is chiefly due to the numerical dissipation

*Corresponding author. *Email address:* zhangbin1983@sjtu.edu.cn (B. Zhang)

 ©2017 Global-Science Press

contained in the schemes, which smears the discontinuity fronts and activates the source terms in a non-physical manner. Since then, this topic has attracted a great deal of attention.

Lafon and Yee [3,4] indicated that the spurious steady state of nonlinear source terms can be linked to the wrong shock speed by getting trapped at one of the stationary solutions, depending on the combination of numerical method, initial data, time step and grid spacing. Griffiths et al. [2] analyzed the different methods of numerically treating the stiff source and their accompanied spurious wave propagation phenomena. Yee et al. [6, 7] followed to investigate the role of CFL playing in the spurious behavior and found the counter-intuitive behavior, which leads to the conclusion that the traditional concept of CFL guideline needs to be revised when extending to the reactive Euler equation systems. Recently, Zhang and Wang [8] give a reasonable explanation that the oscillation of the parameter of an intermediate state which is a decisive factor to decide whether or not the spurious solution will happen, is the likely cause of the counter-intuitive behavior.

Many other researchers focus on designing the new schemes or models to avoid this spurious numerical solution in the under-resolved computational conditions. During the last two decades, several innovative numerical methods, such as the level set and front tracking methods [9–13]; random choice method [14–16]; fractional step method [17]; random projection method (RPM) [18–20]; subcell resolution method [22, 23]; MinMax Method [21]; equilibrium state method (ESM) [24] and many other works [25–31], have been proposed successively. A comprehensive review of the last two decades of this field can be obtained in [22]. In spite of being able to remove or delay the appearance of the spurious solution to some extent, these methods cannot be widely used due to some limitations. For example, existing methods are either confined to a particular flow type or restricted to certain stiffness of the reaction terms. When stiffness of the source term increases, some of the methods would break down even for a single reaction case.

The present work is a sequel to [8] to extend the idea to the Euler equations with stiff detonation. By examining the dissipative discretized counterpart of the Euler equations for a detonation problem consisting of a single reaction, a detail analysis on the spurious wave pattern is presented employing the fractional step method using the Strang splitting. Additionally, a novel method called the threshold values method (TVM for short) is proposed as a modification to the fractional step method with the help of physical arguments. Several single reaction detonation as well as multi-species and multi-reaction detonation test cases with strong stiffness are examined to illustrate the performance of the TVM approach.

## 2 The standard numerical method for the reactive Euler equations

The governing equations are usually used to simulate the inviscid, one-dimensional propagation of a detonation wave, representing conservation of mass, momentum, energy and

species. Consider the simplest reactive Euler equations with only two chemical states which are the burnt gas state and the unburnt gas state:

$$\frac{\partial U}{\partial t}+\frac{\partial F}{\partial x}=S, \tag{2.1}$$

where the vectors contain the conserved variables $U$, flux vector $F$ and the source terms $S$ which convert the unburnt gas to the burnt gas via a single irreversible reaction.

$$U=\begin{pmatrix}\rho\\ \rho u\\ E\\ \rho z\end{pmatrix},\quad F=\begin{pmatrix}\rho u\\ \rho u^2+p\\ u(E+p)\\ \rho z u\end{pmatrix},\quad S=\begin{pmatrix}0\\ 0\\ 0\\ -K(T)\rho z\end{pmatrix}. \tag{2.2}$$

The $\rho$, $u$, $E$ and $z$ are the mixture density, the velocity, the mixture total energy and the mass fraction of the un-burnt gas respectively. The pressure $p$ is given by:

$$p=(\gamma-1)\left(E-\frac{1}{2}\rho u^2-Q_0\rho z\right), \tag{2.3}$$

where $Q_0$ is the chemical heat released in the reaction process. The temperature $T$ is defined as $T=p/\rho$. $K(T)$, the reaction rate of the irreversible chemical process, is expressed in the so-called ignition temperature kinetic [32], which is often used in the chemical reaction with the high-temperature sensitivity and the large activation energies:

$$K(T)=\begin{cases}K_0, & T\geq T_{ig},\\ 0, & T<T_{ig}.\end{cases} \tag{2.4}$$

Due to numerical stability considerations, a common procedure to solve the reactive Euler equations is by the fractional step method using the Strang splitting [33] of the convection and reaction terms (the standard method). In this method, the numerical solution at each time level is computed in two steps: The homogeneous conservation law (i.e., the convection step) and the ODE system (i.e., the reaction step) separately. For example, the numerical solution at time level $t_{n+1}$ is approximated by:

$$U^{n+1}=R(\Delta t)A(\Delta t)U^n. \tag{2.5}$$

The convection operator $A$ is defined to approximate the solution of this problem on the time interval:

$$\frac{\partial U}{\partial t}+\frac{\partial F}{\partial x}=0,\quad t_n\leq t\leq t_{n+1}. \tag{2.6}$$

Based on the MUSCL approach with a TVD Minmod limiter [34], the advection problem is solved numerically with the popular AUSM approach [35,36] by splitting the pressure of the Euler governing equations into two parts, which can be extended to second order. Second order Runge-Kutta time integration [37] is used in time discretization. The

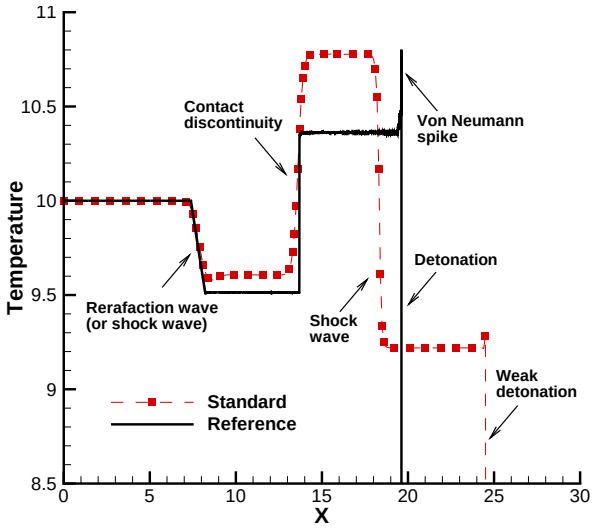


Figure 1: A typical spurious numerical phenomenon compared with the reference ZND solution.

reaction operator $R$ is defined to approximate the solution on a time step of the reaction problem:

$$\frac{dU}{dt}=S, \quad t_n \le t \le t_{n+1}. \tag{2.7}$$

For simplicity, we use the explicit method as the ODE solver in the reaction step since both explicit method and linearized implicit method leads to the spurious behavior [21].

A simple ignition temperature model case solved by the standard method is utilized to show and analyze the characteristics of the spurious numerical phenomenon. We consider an one-dimensional detonation wave propagating with a constant wave speed $S_D$. This problem is solved on the computational domain of $[0,30]$. The initial values consist of the burnt gas on the left-hand side and the unburnt gas on the right-hand side:

$$(\rho,u,p,z)=\begin{cases}(2,2,20,0), & x\le 10,\\ (1,0,1,1), & x>10.\end{cases} \tag{2.8}$$

The $\gamma$, $Q_0$, $K_0$, $T_{ig}$ are 1.4, 20, 10000, 2 respectively. A famous spurious numerical phenomenon may happen if this problem is computed by the standard method in the under-resolved conditions: $N=300$, $\Delta t=0.0001$. On the contrary, a reasonable ZND solution can also be obtained by the standard method with the extremely fine mesh ($N=50000$) and the very small time step ($\Delta t=0.00001$). Compared numerical results at the final time ($t=1.5$) are provided in Fig. 1. We can note that there are several obvious differences between the reference ZND solution and the non-physical solution i.e., nonphysical discrete travelling waves [1]). First, the Von Neumann spike existing in the reference solution cannot be found in the non-physical solution because there are not enough meshes in the reactive zone. Second, there is a bifurcating wave pattern appearing in the incorrect solution: the strong detonation wave changes into a weak detonation wave and a

shock wave. Third, the velocity of the weak detonation wave is larger than that of the shock wave and this implies that the constant state between them will grow gradually as time goes on. Although the spurious solution is the numerical solution of the discretized counterpart but not the physical solution of the original governing Euler equations [1], we may think the shock structures illustrated in spurious behavior as a physical phenomenon since a single discontinuity like weak detonation obeys the Rankine-Hugoniot conditions locally [8]. Thus, we will provide a further explanation of the formation of spurious solution in the stiff reactive Euler equations in a physical view, based on which one may consider a new approach to deal with high stiffness problems as presented in Section 3.

# 3 Modification to standard fractional method: Threshold values method (TVM)

In this section, we will introduce a modification to the standard fractional method, the threshold values method (TVM), by illustrating the formation of spurious behavior as well as the idea of TVM. By solving the exact Riemann problem, TVM procedure applied in a simple reaction problem is presented. Meanwhile, when the exact Riemann solution is absent or includes unsteady initial conditions problems, the extension method is proposed based on the idea of TVM.

## 3.1 Illustration of TVM

The typical spurious solution by standard dissipative method that is represented in Section 2 indicates a faster weak detonation than the following shock in the spurious behavior. However, if we can detect the first grid point that forms the spurious behavior, i.e., the faster weak detonation than shock, then a correction to this grid point can be made, the process of which is detailed as follows.

The detonation wave is smeared within several grid points as the lowercase letters ($a$, $b$, $c$, $d$), which are enclosed by the dashed circles, presenting the pressure, as well as by the dashed triangles, presenting the mass fraction, as illustrated in Fig. 2 (the triangle $a$ and $c$ is overlapped by the triangle $A$ and $C$). The ignition of a grid point must satisfy the temperature that is higher than the ignition temperature $T_{ig}$ and the non-zero mass fraction. Thus, the temperature and pressure at point $b$ has already reached the ignition temperature $T_{ig}$, which means that ignition will occur immediately in the standard dissipative method whereas point $a$, whose mass fraction has decreased to nearly zero (not zero because of numerical viscosity), will no longer increase its temperature due to the ignition.

After a short period $\Delta t$, the temperature of the point $b$ reaches the intermediate state pressure $P^*$ by explicit ODE solver in reaction step $R(\Delta t)$, presented by the point $B^*$. The mass fraction decreases to zero at the same time, which forms the shock structure as indi-

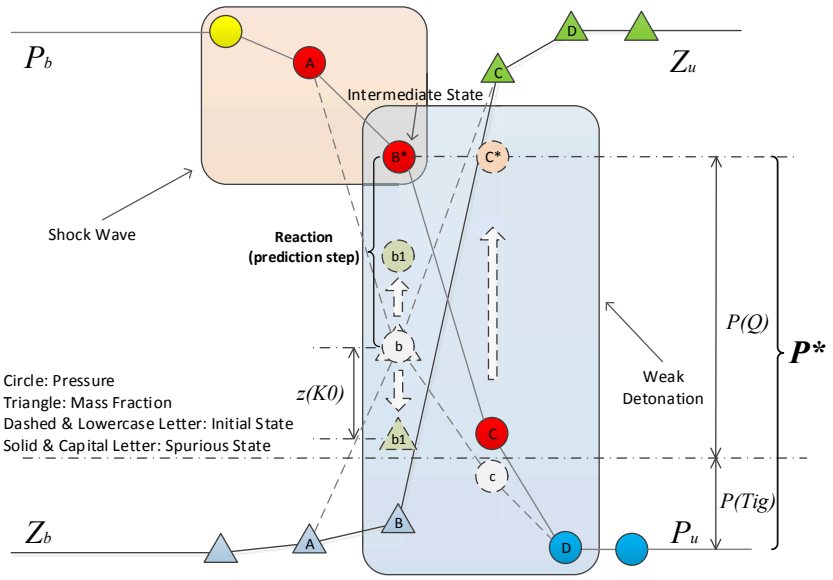


Figure 2: Illustration of the formation for the spurious numerical phenomenon and the idea of TVM. $b$ represents the burnt state and $u$ represents the unburnt state.

cated in Fig. 2. The chemical reaction rate is involved with $K_0$. When $K_0$ is large, point $b$ will react completely to point $B^*$ and mass fraction will decrease to zero with releasing chemical energy ($Q_0$) instantaneously at the same time. However, if $K_0$ is relatively small, point $b$ will arrive to the correct position as shown by point $b1$, which forms the equal speed of shock and detonation that indicate the correct single discontinuity. Point $B$ is the grid point that first reaches the intermediate state, which stimulates the ignition of point $c$ because of the synthesized effect of the advection and the numerical viscosity as shown by point $C$. The variation of mass fraction of point $b$ makes the detonation move forward after the reaction step of point $b$ by the explicit ODE solver. If the weak detonation speed is higher than shock speed at this reaction step, point $C$ will be ignited to the intermediate state similar to point $b$ at the next reaction step, as shown by point $C^*$. Such a scenario leads to the spurious shock structures comprising a weak detonation wave moving forward and a shock wave that travels more slowly behind, as shown by the capital letter points ($A$,$B$,$C$,$D$) enclosed by solid circles and triangles, as indicated in Fig. 2.

If the weak detonation speed ($S_{wd}$) that results from the reacting grid point $b$ to intermediate point $B$ is larger than the corresponding shock wave speed ($S_s$), we can discern this wrong ignited point via an attempt (prediction) by solving the source term in reaction step, as shown in Fig. 2 by the following equation:

$$\begin{cases} \text{if } S_s \geq S_{wd}, & \text{correct ignition,} \\ \text{if } S_s < S_{wd}, & \text{spurious ignition.} \end{cases} \tag{3.1}$$

After the prediction step, each transition point that makes the weak detonation speed

larger than the shock wave speed will be frozen during the reactive step. Thus, calculating the speed of the shock and weak detonation is essential to modifying the standard dissipative method.

### 3.2 Review of [8]: obtain two wave speeds in problems with exact Riemann solutions

Since the shock and weak detonation speed are closely related to burnt state and the unburnt state, it is necessary to obtain the parameters behind and before the detonation (state-4 and 2 in Fig. 3), which turns to solve a reactive Riemann problem in order to calculate these two speeds.

Here, we shortly review the solution method of exact Riemann problem introduced in previous study [8]. As shown in Fig. 3, two theoretical Riemann solutions for Eq. (2.1), consisting of a left wave (either shock or rarefaction), a middle wave which is divided by the contact discontinuity and a right wave of detonation, which are abbreviated to the SCD case and the RCD case separately, will occur, depending on the different initial data, for example that Eq. (2.8) will lead to a RCD case. As we know, relationships exist between the variables on the two sides of a shock wave or a detonation wave. First, we consider the plane of detonation connecting the area 2 and area 4. Detonation Hugoniot

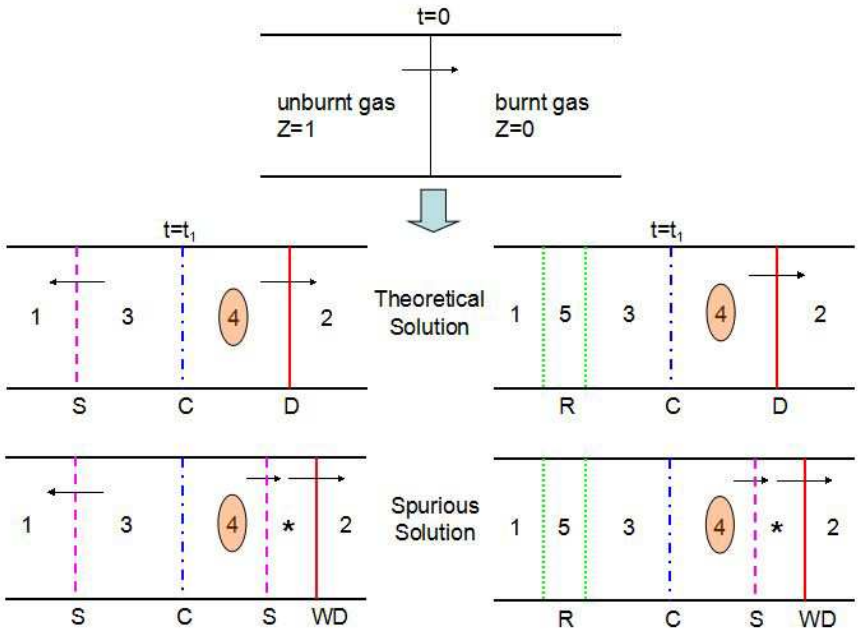


Figure 3: The illustration of theoretical and spurious solution of detonation problem (R short for rarefaction wave; S short for shock wave; C short for contact discontinuity; D short for detonation wave; WD short for weak detonation wave; *-state is the transition point that ignited after prediction step in reaction solver).

equations are given as follows:

$$\begin{cases} \rho_2(S_D-u_2)=\rho_4(S_D-u_4), \\ p_4-p_2=\rho_2(S_D-u_2)(u_4-u_2), \\ \dfrac{p_4}{\rho_4(\gamma-1)}-\dfrac{p_2}{\rho_2(\gamma-1)}=\dfrac{1}{2}(p_2+p_4)\left(\dfrac{1}{\rho_2}-\dfrac{1}{\rho_4}\right)+Q_0. \end{cases} \tag{3.2}$$

Set the $p_4$ as a known variable, we can get the expression of $u_4$ by solving Eq. (3.2):

$$u_4-u_2=\sqrt{\frac{2(p_4-p_2)(p_4-p_2-(\gamma-1)\rho_2Q_0)}{\rho_2[(\gamma+1)p_4+(\gamma-1)p_2]}}=-f(p_4,p_2,\rho_2,Q_0). \tag{3.3}$$

If $p_3>p_1$, there will be a shock wave on the left side. Eq. (3.4) shows the relationships of variables on the two sides of the shock wave:

$$\begin{cases} \rho_1(S_S-u_1)=\rho_3(S_S-u_3), \\ p_3-p_1=\rho_1(S_S-u_1)(u_3-u_1), \\ \dfrac{p_3}{\rho_3(\gamma-1)}-\dfrac{p_1}{\rho_1(\gamma-1)}=\dfrac{1}{2}(p_1+p_3)\left(\dfrac{1}{\rho_1}-\dfrac{1}{\rho_3}\right). \end{cases} \tag{3.4}$$

A similar treatment to Eq. (3.4) and a expression of $u_3$ are obtained:

$$u_3-u_1=-\frac{p_3-p_1}{\sqrt{\frac{\rho_1[(\gamma+1)p_3+(\gamma-1)p_1]}{2}}}=-g_S(p_3,p_1,\rho_1). \tag{3.5}$$

If $p_3<p_1$, a rarefaction wave will form on the left side. We can also get a similar expression of $u_3$ with two additional equations. The first one is the equation of Riemann invariants:

$$u_1+\frac{2c_1}{\gamma-1}=u_3+\frac{2c_3}{\gamma-1}, \tag{3.6}$$

where $c$ is the sound speed and can be computed by:

$$c=\sqrt{\frac{\gamma p}{\rho}}. \tag{3.7}$$

The other one is the isentropic relation in rarefaction wave:

$$\frac{p_1}{\rho_1^\gamma}=\frac{p_3}{\rho_3^\gamma}. \tag{3.8}$$

The expression of $u_3$ for a rarefaction wave is given as follows:

$$u_3-u_1=-\frac{2c_1}{\gamma-1}\left[\left(\frac{p_3}{p_1}\right)^{\frac{\gamma-1}{2\gamma}}-1\right]=-g_R(p_3,p_1,\rho_1). \tag{3.9}$$

If set $p_3=p_1$, one can discern the RCD from SCD case by comparing the magnitude of release heat $Q_0$ with the critical release heat $Q_{cr}$:

$$\begin{aligned} &u_2-u_1=f(p_3,p_2,\rho_2,Q_{cr})=f(p_1,p_2,\rho_2,Q_{cr}) \\ \Rightarrow &Q_{cr}=\frac{p_1-p_2}{\gamma-1}-\frac{(u_2-u_1)^2[(\gamma+1)p_1+(\gamma-1)p_2]}{2(p_1-p_2)(\gamma-1)}. \end{aligned} \tag{3.10}$$

If initial value $Q_0$ is greater than $Q_{cr}$, then $p_3>p_1$, which means the SCD case and vice versa. Considering that the middle state is split into area 3 and area 4 by a contact discontinuity, we have $u_3=u_4$ and $p_3=p_4$. The following equation results from subtracting Eq. (3.3) from Eqs. (3.5) or (3.9) if the calculating case is determined as SCD or RCD case:

$$\begin{cases} u_2-u_1=-g_{\mathrm{S}}(p_3,p_1,\rho_1)+f(p_3,p_2,\rho_2,Q_0), & \text{SCD case,} \\ u_2-u_1=-g_{\mathrm{R}}(p_3,p_1,\rho_1)+f(p_3,p_2,\rho_2,Q_0), & \text{RCD case.} \end{cases} \tag{3.11}$$

We can compute $p_3$ by using Newton iteration method to solve Eq. (3.11). Then other parameters ($u_3$,$\rho_3$) behind the detonation can be obtained easily. The corresponding $S_s$ and $S_{wd}$ for each transition point can be expressed as the following Eq. (3.12) by using momentum equation in Eqs. (3.2) and (3.4). The heuristic diagram is shown in Fig. 3

$$\begin{cases} S_s=u^*+\dfrac{p_4-p^*}{\rho^*(u_4-u^*)}, \\ S_{wd}=u_2+\dfrac{p^*-p_2}{\rho_2(u^*-u_2)}. \end{cases} \tag{3.12}$$

One thing needs to be noticed is that when $u^*$ is very close to $u_4$, the shock speed is set to larger than the weak detonation speed to avoid the singularity result in calculating the shock speed.

## 3.3 TVM introduction

### 3.3.1 TVM for reaction with exact Riemann solution

If the parameters $p_4$ and $u_4$ of exact Riemann solution can be calculated, then several modifications of the standard method to achieve the correct shock speed can be made:

(1) Parameters behind the detonation are confirmed by solving an exact Riemann problem in the initialization step, which determines $p_4$ and $u_4$ in Eq. (3.12). $\rho_2$, $p_2$, and $u_2$ equal to unburnt parameters.

(2) Temporary mass fraction consumption of transition points that satisfy $T^*>T_{ig}$ are obtained by solving the source terms by the explicit ODE method, which is the first step of the method termed as ***Predictor*** $U_i^*$ to obtain the intermediate state parameters $p^*$, $\rho^*$, and $u^*$, as shown in Fig. 3:

$$U_i^*=R(\Delta t)U_i^n. \tag{3.13}$$

In the predictor, $p^*$ is updated by Eq. (2.3). $\rho^*$ and $u^*$ do not update in the prediction step and are equal to the local density and velocity because of the mass conservation in the reaction operator. Thus, the speed of shock $S_s$ and weak detonation $S_{wd}$ can be calculated by Eq. (3.12).

(3) After the predictor, those transition points ($T^* > T_{ig}$) that satisfy $S_s \geq S_{wd}$ in Eq. (3.1) will be allowed to ignite in the reaction operator, which is called the second step of the method termed as **Corrector**:

$$U_i^{**} = \begin{cases} U_i^*, & \text{if } S_s \geq S_{wd}, \\ U_i^n, & \text{if } S_s < S_{wd}. \end{cases} \tag{3.14}$$

(4) Finally, the conservation variables are normally updated by the advection operator in normal way after the reaction operator is corrected by the wave speed relation:

$$U_i^{n+1} = A(\Delta t) U_i^{**}. \tag{3.15}$$

This proposed method is called the threshold values method because whether these transition points ($T^* > T_{ig}$) will be ignited or not all depend on a set of threshold parameters ($p^*, u^*, \rho^*$). TVM can prevent the spurious numerical phenomena from appearing even in the under-resolved conditions. This advantage will be proven by many simple reaction test cases.

### 3.3.2 TVM for reaction without exact Riemann solution

As shown in Eq. (3.12), the shock speed and the weak detonation speed can be calculated without the exact solution of the Riemann problem if the unknown parameters $p_4$ and $u_4$ (as well as 2-state parameters $p_2$, $u_2$ and $\rho_2$ in such cases as unsteady initial conditions are concerned) can be obtained, thereby indicating that the method can be extended to more complicated problems such as multi-species, multi-reaction cases, and the unsteady initial condition problems. Therefore, the key to the extension of TVM is to determine the concerned parameters $p_4$ and $u_4$ after the detonation and the 2-state parameters $p_2$, $\rho_2$, and $u_2$ before detonation. In the following paragraph, a kind of mass fraction detector is introduced and applied to determine the concerned parameters.

**TVM for unsteady initial conditions problems and multi-species problems**

If the unsteady state is considered, the parameters concerned such as $p_4$ and $u_4$ are approximated as the pressure and velocity in the transition points whose mass fraction is not zero (in all cases, $|z|<10^{-2}$). The mass fraction detector works well in all cases because the corresponding $p_4$ and $u_4$ are updated from the similar status of point $A$ in Fig. 2 since it is the exact point in front of the ignition grid point similar to point $B$. Accordingly, if one parameter before detonation front is unsteady such as density in the example of Section 5.1, then $\rho_2$ is found in the transition point similar to point $D$ ($|z-1|<10^{-2}$) in Fig. 2 because it is the point that connects the ignition point in the prediction step to form the weak detonation structure.

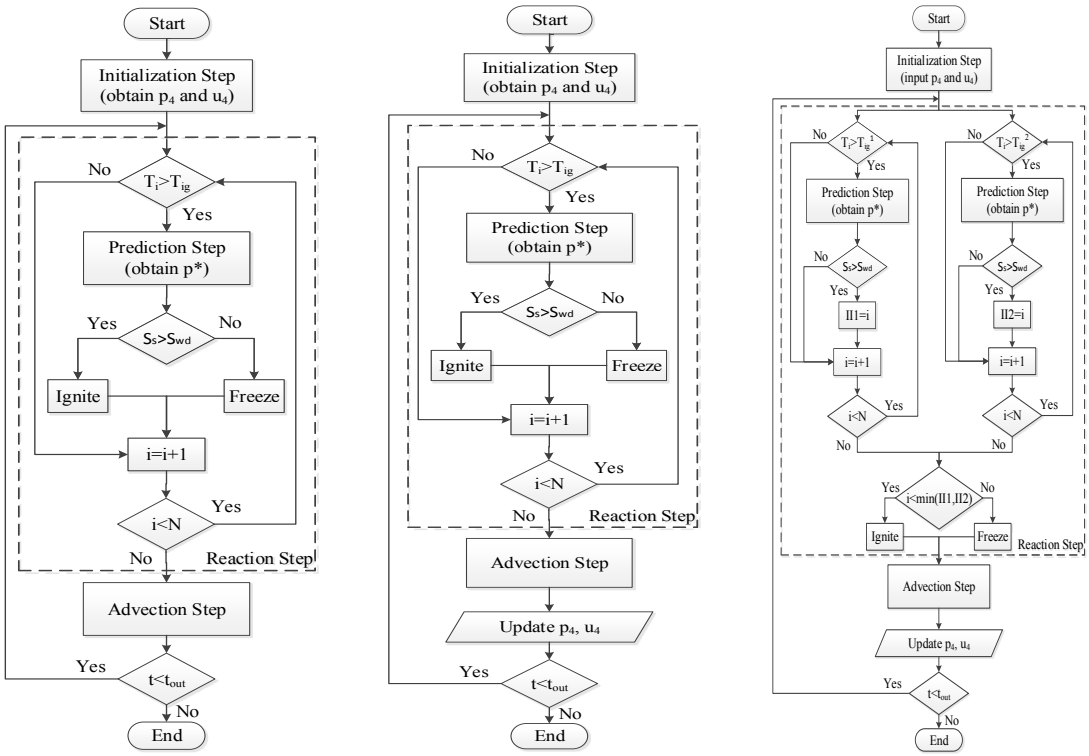


(a) TVM for simple reaction problems

(b) TVM for unsteady initial conditions problems and multi-species problems

(c) TVM for multi-reaction problems

Figure 4: Summarized flow chart of TVM for different reaction problems. $i$ represents the index of the grid points and $N$ is the number of the grid points.

(5) Mass fraction detector in TVM for complicated problems: post-detonation parameters $p_4$ and $u_4$ are updated from the transition point that satisfies $|z|<10^{-2}$. The initialization of $p_4$ and $u_4$ is chosen as the post-detonation parameters of the initial conditions. The initialization step and update step for $p_4$ and $u_4$ are plotted in the flow charts of Fig. 4.

In the multi-species problems with only one reaction, the calculation steps are similar to the TVM for unsteady initial condition cases. One minor revision is necessary, which is that $p_4$ and $u_4$ are updated from the transition point that satisfies $|z_{\text{fuel}}|<10^{-2}$. Such as in the $H_2$ and $O_2$ one-step chemical reaction introduced in Section 5.2, the 4-state parameters are found in the transition point whose mass fraction of $H_2$ satisfies $|z_{H_2}|<10^{-2}$.

**TVM for multi-reaction problems**

Although TVM can correctly restrain the wrong detonation wave, over-restraint can occur in the transition points in multi-reactions, which makes the mass fraction of fuel not consume correctly. Thus, in the reaction operator, the predictor of different reactions

are calculated separately to get a detonation front whose position satisfies $S_s > S_{wd}$ in Eq. (3.1). Then, as shown in Fig. 4(c), the true detonation front position is obtained by choosing the smallest position of detonation front calculated from different reactions. Once the detonation front is determined, the source term is solved again via a standard implicit solver in the region after the detonation front position. The choice of 4-state parameters $p_4$ and $u_4$ is same as the one in multi-species cases as introduced above.

(6) The corrector in reaction operator in multi-reaction problems is to get the true detonation front position $II_{\text{front}}$ ($II$ is the index number of the grid points and the detonation is assumed to propagate in the direction to the large index number):

$$II_{\text{front}} = \min_j II_j, \quad j = 1, \cdots NR, \tag{3.16}$$

where grid point $II_j$ is the maximum grid point that satisfies $T > T_{ig}^j$ and $S_s > S_{wd}$ ($T_{ig}^j$ is the ignition temperature of the $j$th reaction). Then reaction operator is solved by the standard method in the grid points that are smaller than $II_{\text{front}}$:

$$U_i^{**} = R(\Delta t) U_i^n, \quad i = 1, \cdots II_{\text{front}}. \tag{3.17}$$

In summary, several extensions are made based on the idea of TVM and the calculation rules are summarized in Fig. 4. High order spatial discretization schemes will resolve the spurious behavior to some extent [22, 23], although spurious behavior will persist in certain realistic extreme flow conditions [38]. However, faster propagation of spurious detonation will be restrained by TVM as long as the spurious bifurcating shock structures occur because TVM only modifies the source operator, not the advection operator as related above. Such a scenario indicates that TVM can be used both in splitting scheme and in other high-order schemes; furthermore, TVM will have the potential to simulate the extreme flow conditions such as those described in [38].

# 4 Simple reaction examples with extreme conditions

This section presents the performance of the proposed method for four simple reaction test cases. In order to illuminate the characteristic of the threshold values method, TVM is compared by ESM method [24] and MinMax method [21]. In the first example, the RCD and SCD cases are numerically simulated by four different methods whose results are compared to the reference solution. In the following three examples, the effects of three important parameters as related in Section 3.3 i.e., the chemical reaction rate $K_0$, the ignition of temperature $T_{ig}$ and the release heat $Q_0$ are assessed on the appearance of the spurious solution by the different methods.

## 4.1 Example 1: The standard case

Different initial data will lead to different Riemann solutions. In this example, two initial data are chosen to obtain the RCD case and the SCD case respectively. All initial val-

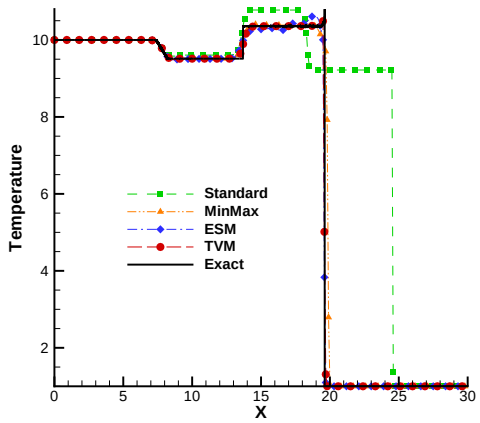


(a) RCD case of different methods

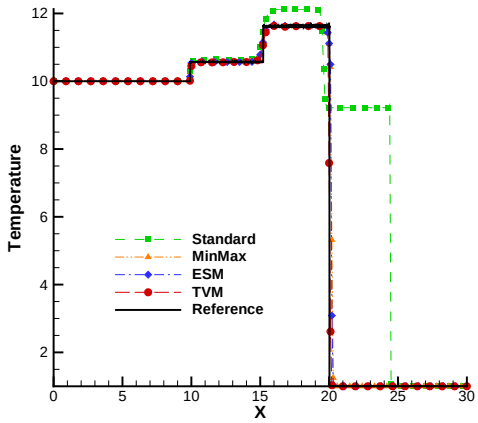


(b) SCD case of different methods

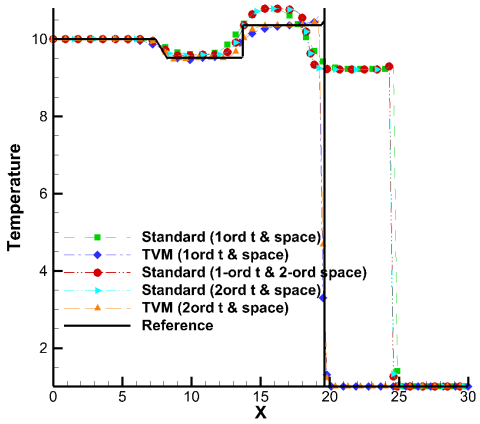


(c) RCD case of different discretizations

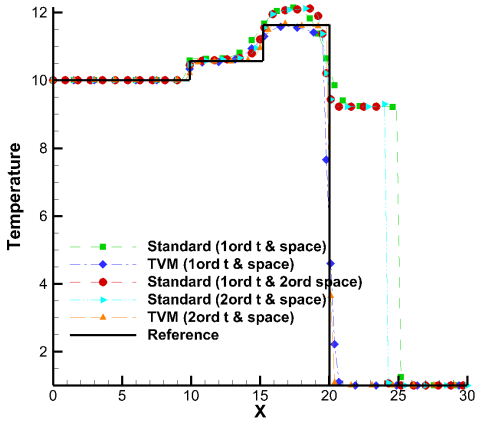


(d) SCD case of different discretizations

Figure 5: Numerical results for standard case by different spacial/temporal discretizations and different methods.

ues and important parameters for the RCD case are the same as Eq. (2.8), except that the parameter $u$ on the left side of the calculation area in Eq. (2.8) is 4 in the SCD case. Reference solution is solved by the standard method with 50000 grid points and extremely small time step of 0.000001. Much less grid number which is 300 and larger time step which is 0.0001 are considered in all four methods.

As represented in Figs. 5(a) and (b), all modified methods can restrain the spurious behavior and reach the correct solution contrary to the spurious numerical solution by the standard dissipative method in the conditions of the same number of gird points and the same time step. Considering the similar shock patterns in the RCD and SCD cases, all numerical test cases in the following three examples will be the SCD case (RCD: $p_4=16.796$ and $u_4=2.4609$; SCD: $p_4=24.2456$ and $u_4=3.4784$ in TVM calculation).

The spacial discretization and temporal integration can effect the spurious behavior [3, 4], which are represented in Figs. 5(c) and (d). The grid number of all cases are decreased to 100 for comparison of spurious behavior of different schemes. However, temporal discretization effect is small and higher spatial discretization obtains a less spurious behavior as shown in Figs. 5(c) and (d), which indicates the higher discretization method cannot solve the spurious problem but only soothe the phenomena [8]. Thus all numerical test cases in the following examples will be solved in first order temporal and second order spacial discretization.

## 4.2 Example 2: Chemical reaction rate ($K_0$)

The manner in which the chemical reaction rate $K_0$ is chosen can affect the level of the spurious behavior in the advection-reaction problems ($Q_0 = 20$ and $T_{ig} = 2$). As can be seen in Fig. 6(a), except in $K_0 = 100$ (representing the lower stiffness) showing a correct solution, all other $K_0$ conditions lead to the spurious phenomenon solved by the standard dissipative method. Besides, with the larger $K0$ (representing the higher stiffness), the spurious behavior comes to appear more obvious. However, the degree of spurious behavior seems to be the same when $K_0 = 10000$ and $K_0 = 15000$.

As illustrated in Fig. 6(b), all ameliorated methods mentioned above give the precise solution referring to the reference solution when the chosen $K_0$ is equal to 15000, which is contrary to the solution by the standard dissipative method, showing a bifurcating wave pattern ($p_4 = 24.2456$ and $u_4 = 3.4784$ in TVM calculation).

The difference of the shock wave speed and the weak detonation wave speed $DS$ with the growth of the chemical reaction rate $K_0$ is represented in Fig. 7. If $K_0$ is smaller than

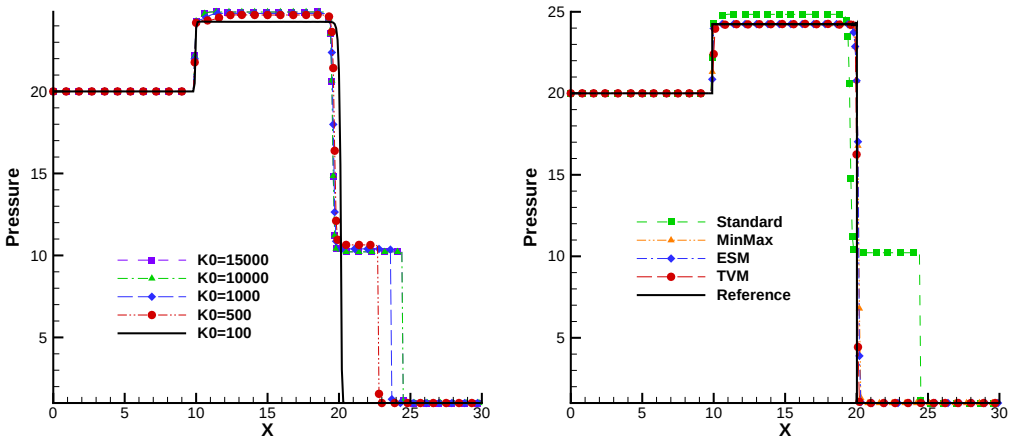


(a) The results of standard dissipative method at different $K0$

(b) The results of different methods at $K0 = 15000$

Figure 6: Numerical results for ratio of chemical process.

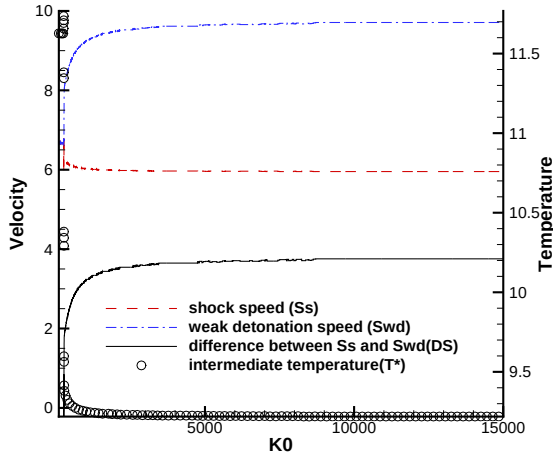


Figure 7: Intermediate state parameters with varying $K0$.

200, the spurious phenomenon will not appear for the quicker speed of the shock wave. When $K_0$ increases, the mass fraction of a transition point will decrease precipitately, which generates a faster weak detonation wave movement. However, as $K_0$ reaches to an extremely high value (approximately equal to 5000), the difference between the shock wave speed and the weak detonation wave speed $DS$ converges to a constant, which means the numerical solution will become the same spurious degree as shown in Fig. 6(a) in the high $K_0$ conditions. The reason for this phenomenon is that when $K_0$ is larger than an extreme value, the ignited transition point will get to the equilibrium state in one time step and release chemical heat immediately, which leads to the constant weak detonation wave speed as illustrated in Section 3.1.

### 4.3 Example 3: Ignition temperature ($T_{ig}$)

The main emphasis in this example is to study the influence of different ignition temperatures in the behavior of spurious numerical solution of the SCD case ($K_0 = 10000$ and $Q_0 = 20$). As shown in Fig. 8(a), the numerical solution solved by standard dissipative method tends to be more spurious (the gap between the shock wave and the weak detonation wave gradually enlarges) with the smaller $T_{ig}$ between five ignition temperatures.

In view of the different modified methods, the ignition temperature equal to 1.1 at which spurious behavior is most likely to happen is treated by four different methods as demonstrated in Fig. 8(b). Standard dissipative method solving this extreme case gives a typical spurious solution as expected. On the contrary, the TVM method offer an accurate result as the reference solution presented. Although the ESM method gives a wrong shock pattern in settling this case, the degree of the spurious phenomenon of ESM seems less than the one of the standard dissipative method. MinMax method seems robust in the extreme ignition temperature problems ($p_4 = 24.2456$ and $u_4 = 3.4784$ in TVM calculation).

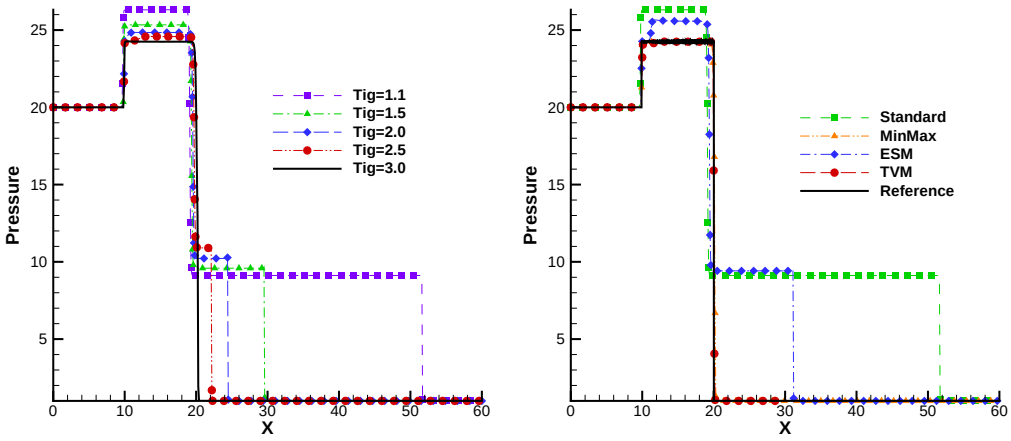


(a) The results of standard method at different $T_{ig}$

(b) The results of different methods at $T_{ig}=1.1$

Figure 8: Numerical results for ignition temperature.

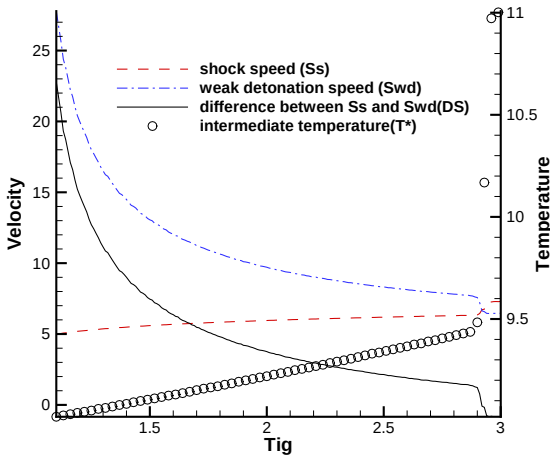


Figure 9: Intermediate state parameters with varying $T_{ig}$.

For clarity of the presentation of the influence of the ignition temperature $T_{ig}$ on the spurious behavior, the intermediate temperature $T^*$ and the discrepancy between shock speed $S_s$ and weak detonation speed $S_{wd}$, i.e., $DS=S_{wd}-S_s$ are plotted against the 200 ignition temperature conditions (from $T_{ig}=1.1$ to $T_{ig}=3$ and $\Delta T_{ig}=0.01$) as shown in Fig. 9. As ignition temperature increases, the shock velocity rises gradually making $DS$ diminish to nearly zero; meanwhile, the intermediate temperature increases linearly. Besides, the standard dissipative method will give a correct solution in the conditions of $T_{ig}>2.9$ for the shock wave will move faster than the weak detonation wave. However, when

the ignition temperature is extremely low, more intermediate state points whose temperatures are higher than the ignition temperature will be ignited wrongly to the spurious state.

### 4.4 Example 4: Release heat ($Q_0$)

Fig. 10(a) gives the contrast between the solutions solved by the standard dissipative method with four different release heat $Q_0$ ($K_0=10000$ and $T_{ig}=2$). Only when $Q_0=15$, the standard dissipative method shows a correct solution. All other three release heat conditions give the spurious solutions by the standard dissipative method. Besides, the higher release heat generates a more spurious solution.

Contrast of different methods to solve $Q_0=30$ case demonstrated in Fig. 10(b) shows up some key differences. The most striking phenomenon is the comparison between the standard dissipative method, ESM and MinMax method, all of which generate the similar spurious pattern. Although ESM gives an erroneous solution likewise, the degree of spurious behavior by ESM is much smaller than MinMax and the standard dissipative method. However, the proposed TVM method gets us the correct solution in the under-resolved conditions as the reference solution ($p_4=26.2914$ and $u_4=3.2546$ in TVM calculation).

With respect to the specific influence caused by $Q_0$, the variation of shock wave velocity, weak detonation velocity and intermediate temperature with the change of parameter $Q_0$ (from $Q_0=10$ to $Q_0=30$ and $\Delta Q_0=0.1$) is demonstrated in Fig. 11. We can find that if $Q_0<16$, the spurious behavior will not happen because of the higher shock wave speed than the weak detonation wave speed. However, when $Q_0>16$, the velocity of the weak detonation and the intermediate temperature increases linearly as the shock velocity re-

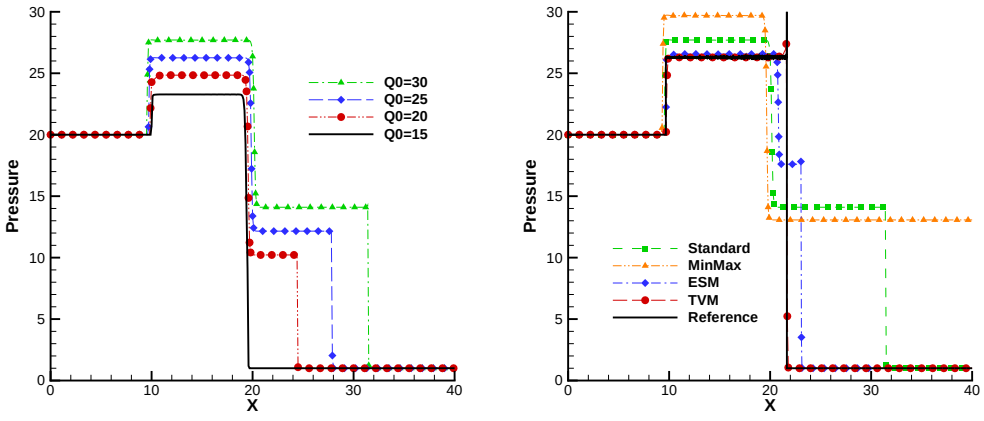


(a) The results of standard dissipative method at different $Q_0$

(b) The results of different methods at $Q_0=30$

Figure 10: Numerical results for release heat.

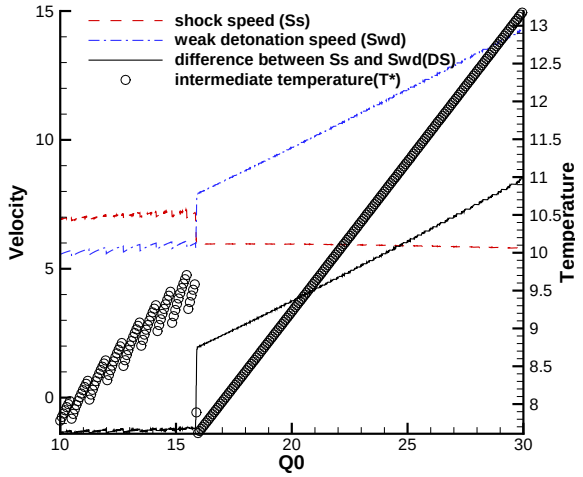


Figure 11: Intermediate state parameters with varying $Q_0$.

mains the constant, which contributes to a larger difference between the weak detonation wave speed and the shock wave speed and thus means a more obvious spurious solution.

### 4.5 Summary

The simple reaction cases indicate that three important parameters i.e., $K_0$, $T_{ig}$ and $Q_0$) that also appear in the illustration of TVM are vital for the occurrence of spurious solution. Traditionally, spurious behavior is believed to happen more easily under strong stiffness, in which chemical reaction rate $K_0$ is large. However, the case of different chemical reactions indicates that when large chemical reaction rate is considered, no more spurious behavior will occur and ESM method can easily represent the single discontinuity. The effect of $K_0$ is even smaller than those of $T_{ig}$ and $Q_0$, thereby indicating that the spurious behavior is not just related to chemical reaction rate, but is also strongly related to the ignition temperature and heat release from the reaction.

## 5 Extension to more complicated problems

### 5.1 Problems with complex initial conditions

The first example uses Heaviside model and has been studied in [22] but with the stronger stiffness. This one-dimensional detonation problem involves a collision with an oscillatory wave in density. The computational domain is $[0,2\pi]$ and the initial conditions are given as follows:

$$(\rho,u,p,z)=\begin{cases}(2,4,40,0), & x\leq\dfrac{\pi}{2},\\ (1.0+0.5\sin 2x,0,1,1), & x>\dfrac{\pi}{2}.\end{cases} \tag{5.1}$$

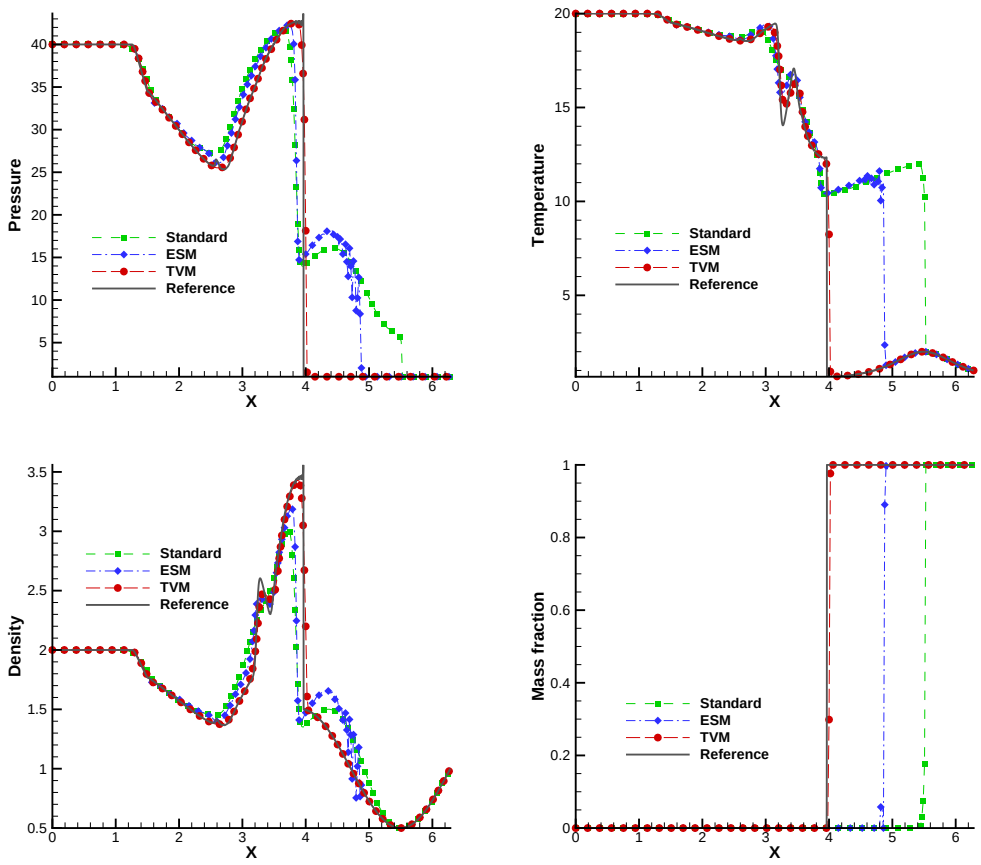


Figure 12: Computed results for unsteady initial conditions case at $t=\pi/10$. All methods with $N=300$ except for reference solution with $N=10000$ by standard dissipative method.

The strong stiffness parameters are given by:

$$(\gamma, T_{ig}, K_0, Q_0) = (1.2, 2, 4000, 50). \tag{5.2}$$

The chemical reaction rate is set higher than the one in [22,24], which makes the problem more stiff and the spurious behavior will happen more easily. The reference solution is solved by the standard splitting method with refined mesh ($N=10000$) and $CFL=0.5$. The numerically solved pressure, temperature, density and mass fraction are plotted in Fig. 12, where results solved by ESM, the standard dissipative method as well as TVM with the same coarse mesh ($N=300$) and $CFL=0.1$ are also displayed. Although the unsteadiness and the absence of exact Riemann solution, TVM obtains the correct solution as reference results, which shows the robustness of TVM in strong stiffness problem.

The second example is the initial conditions that involves with the detonation colliding with a rarefaction wave, which is also been studied in [22, 24]. The computational

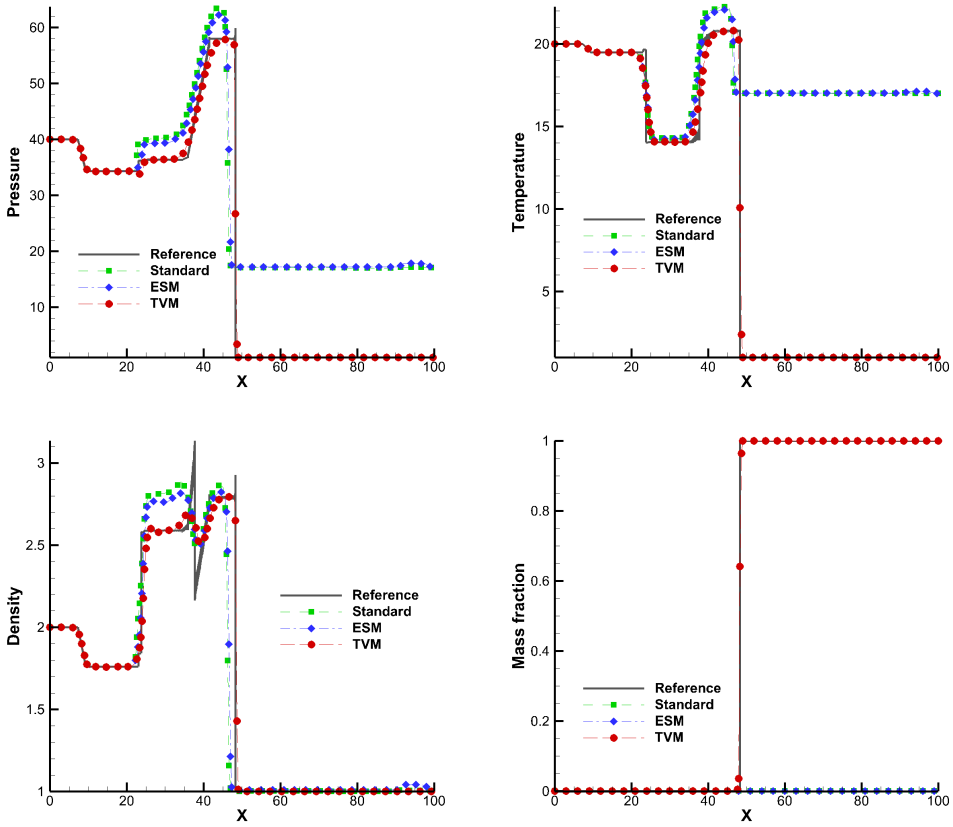


Figure 13: Computed results for unsteady initial conditions case at $t=3$. All methods with $N=300$ except for reference solution with $N=250000$ by standard dissipative method.

domain is $[0,100]$ and the initial conditions are:

$$(\rho,u,p,z)=\begin{cases}(2,4,40,0), & x\leq 10,\\ (3.6428,6.2489,54.8244,0), & 10<x\leq 20,\\ (1,0,1,1), & x>20.\end{cases} \tag{5.3}$$

The parameters are chosen as:

$$(\gamma,T_{ig},K_0,Q_0)=(1.2,1.02,10000,80). \tag{5.4}$$

The ignition temperature is lower, chemical reaction rate and release heat are higher than those in [22, 24]. The reference solution is solved by the standard splitting method with refined mesh ($N=250000$) and $CFL=0.7$. As comparison, the results solved by ESM, standard method and TVM with the same coarse mesh ($N=300$) and $CFL=0.04$ are also displayed in Fig. 13. It can be found that TVM obtains the correct detonation discontinuity. However, results solved by ESM and standard dissipative method give the classical bifurcating wave structures.

### 5.2 Multi-species problem

In the following paper, the multi-species and multi-reaction cases are considered. Thus the calculation method is necessary to be introduced. The governing equations of multi-species and multi-reaction problems are similar as the ones in [24]. Elementary irreversible reactions involving $NS$ species can be represented in the following form:

$$\sum_{i=1}^{NS} v'_{i,j}\chi_i \Longleftrightarrow \sum_{i=1}^{NS} v''_{i,j}\chi_i, \quad j=1,\cdots NR, \tag{5.5}$$

where $NR$ is the number of reactions. The stoichiometric coefficients $v$ are integer numbers and $\chi_i$ is the chemical symbol for the $i$th species. The superscript $'$ indicates forward stoichiometric coefficients, while $''$ indicates reverse stoichiometric coefficients. The production rate $\omega_i$ of the $i$th species can be calculated as a summation of the rate of progress variables for all reactions involving the $i$th species:

$$\omega_i = W_i \sum_{j=1}^{NR} (v''_{i,j} - v'_{i,j}) K_j \prod_{i=1}^{NS} \left(\frac{\rho z_i}{W_i}\right)^{v'_{i,j}}, \quad j=1,\cdots NR, \tag{5.6}$$

where $W$ is the molecular weight. $K_j$ is the reaction rate of the irreversible chemical reaction of the $j$th reaction which is expressed in Heaviside form. The standard method still uses the Strang splitting and AUSM with TVD minmod limiter as the convection operator in the multi-species Euler problems. A full implicit scheme is applied to update the source term, which is different from the reaction operator in the simplest Euler equations:

$$U^{n+1} = U^n + \frac{\Delta t S}{1-\Delta t S'}, \tag{5.7}$$

where $S'$ is the Jacobian of the reaction source term and can be expressed as:

$$S' = \frac{\partial S}{\partial U} = \begin{pmatrix} \dfrac{\partial \omega_1}{\partial(\rho z_1)} & \cdots & \dfrac{\partial \omega_1}{\partial(\rho z_{NS})} \\ \vdots & \ddots & \vdots \\ \dfrac{\partial \omega_{NS}}{\partial(\rho z_1)} & \cdots & \dfrac{\partial \omega_{NS}}{\partial(\rho z_{NS})} \end{pmatrix}. \tag{5.8}$$

LU decomposition is used to solve Eq. (5.7).

A simple reacting model (three species and one reaction equation) is considered in multi-species example. Similar case had been investigated in [20]. The reaction equation is:

$$2H_2 + O_2 \rightarrow 2H_2O. \tag{5.9}$$

The necessary parameters are presented as follows:

$$(\gamma, T_{ig}, K_0, Q_{H_2}, Q_{O_2}, Q_{H_2O}, W_{H_2}, W_{O_2}, W_{H_2O}) = (1.4, 2, 10^6, 600, 0, 0, 2, 32, 18). \tag{5.10}$$

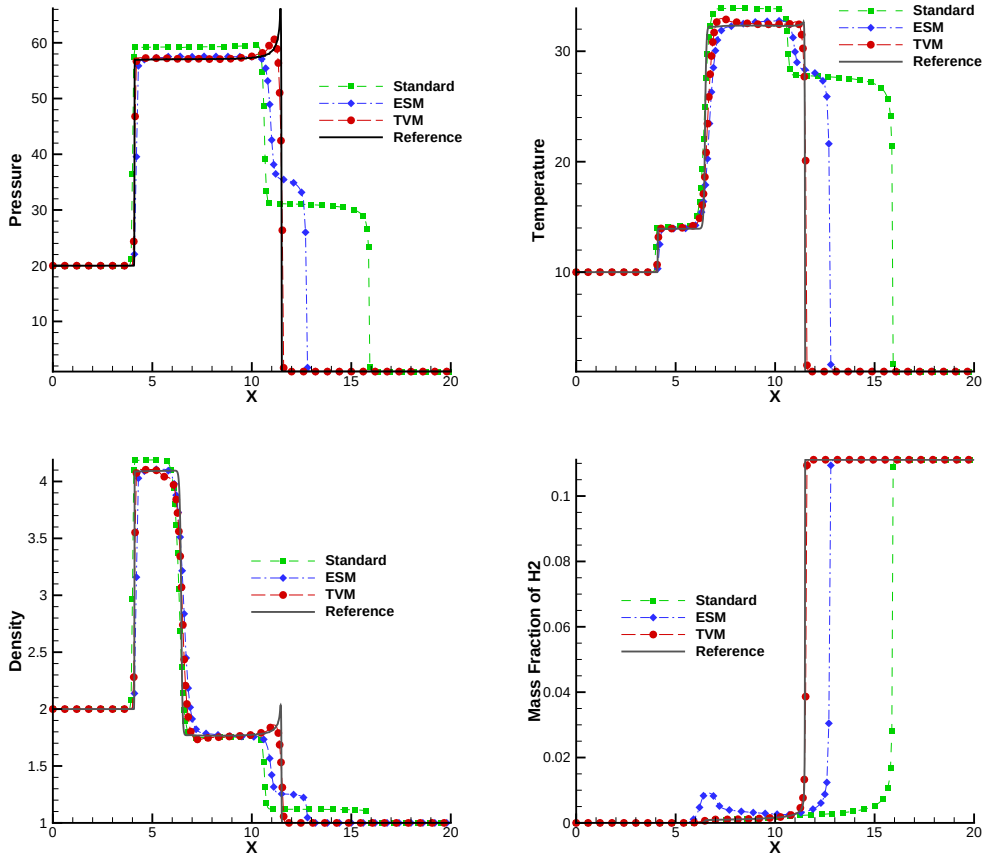


Figure 14: Computed results for multi-species case at $t=0.8$. All methods with $N=300$ except for reference solution with $N=2000$ by standard dissipative method.

The release heat of $H_2$ is set higher to than the one in [20, 24] which makes an extreme condition that more spurious behavior will occur as in simple reaction cases. The initial data consist of the burnt gas on the left side and the unburnt gas on the right side. This problem is solved on the interval $[0,20]$. The initial data are piecewise constants given by:

$$(\rho,u,p,z_{H_2},z_{O_2},z_{H_2O})=\begin{cases}(2,8,20,0,0,1), & x\leq 2.5,\\ (1,0,1,1/9,8/9,0), & x>2.5.\end{cases} \tag{5.11}$$

The reference solution is obtained by the standard splitting method with refined mesh ($N=2000$) and $CFL=0.1$. The reference solution consists of a detonation wave, followed by a contact discontinuity and a shock as shown in Fig. 14. The numerical results by ESM, the standard dissipative method as well as TVM with the same coarse mesh ($N=300$) and $CFL=0.1$ are also displayed. Different parameters of the results with different schemes are plotted in Fig. 14. In this extreme condition, ESM and standard splitting method both

illustrate the spurious behavior as expected. However, TVM gives the same detonation wave speed as the reference solution.

### 5.3 Multi-reaction problem

In multi-reaction problem, a reacting model which consists of five species and two reactions is considered as:

$$H_2+O_2\to 2OH,\quad 2OH+H_2\to 2H_2O. \tag{5.12}$$

The species $N_2$ is treated as a catalyst. Similar example was investigated in [24]. All parameters used in computation are set to the condition of both stiff reactions, given as follows:

$$\begin{cases} (\gamma,T_{ig}^1,K_0^1,T_{ig}^2,K_0^2)=(1.4,1.5,10^5,1.5,10^5),\\ (Q_{H_2},Q_{O_2},Q_{OH},Q_{H_2O},Q_{N_2})=(0,0,-100,-100,0),\\ (W_{H_2},W_{O_2},W_{OH},W_{H_2O},W_{N_2})=(2,32,17,18,28). \end{cases} \tag{5.13}$$

The initial conditions are given as follows:

$$(\rho,u,p,z_{H_2},z_{O_2},z_{OH},z_{H_2O},z_{N_2})=\begin{cases} (2,10,40,0,0,0.17,0.63,0.2), & x\le 0.5,\\ (1,0,1,0.08,0.72,0,0,0.2), & x>0.5. \end{cases} \tag{5.14}$$

Fig. 15 indicates the numerical solutions by the proposed method with the coarse mesh ($N=300$) on the interval $[0,2]$ and $CFL=0.1$. Refined mesh ($N=4000$) and $CFL=0.1$ are applied by the standard method to obtain the reference solutions. In this bi-stiff reaction system, ESM gives the typical spurious solutions as the ones by standard splitting method. However, the same wave patterns with the correct speeds are captured by TVM referring to the reference solutions. Only a short simulation time is offered since the reference solution breaks down to spurious bifurcating solutions at late time due to the strong stiffness. However, the proposed method gives the correct single detonation front at late time, which is not shown in this figure.

## 6 Concluding remarks

Spurious solution by the standard dissipative method will occur in the conditions of the coarse grid and large time scale when simulating stiff reactive problems. Detailed analysis on the formation of spurious wave pattern is presented that uses the standard fractional step method using Strang splitting. With the help of physical arguments, this paper concentrates on devising a modification to standard fractional method, threshold values method (TVM), which can eliminate spurious behavior both in one-reaction and multi-reaction problems with strong stiffness. Single reaction detonation as well as multi-species and multi-reaction detonation test cases are examined to demonstrate the superiority of the TVM approach in general. Extension of TVM to multi-dimensional problems can be developed by choosing the proper post detonation parameters and will be the focus of future work.

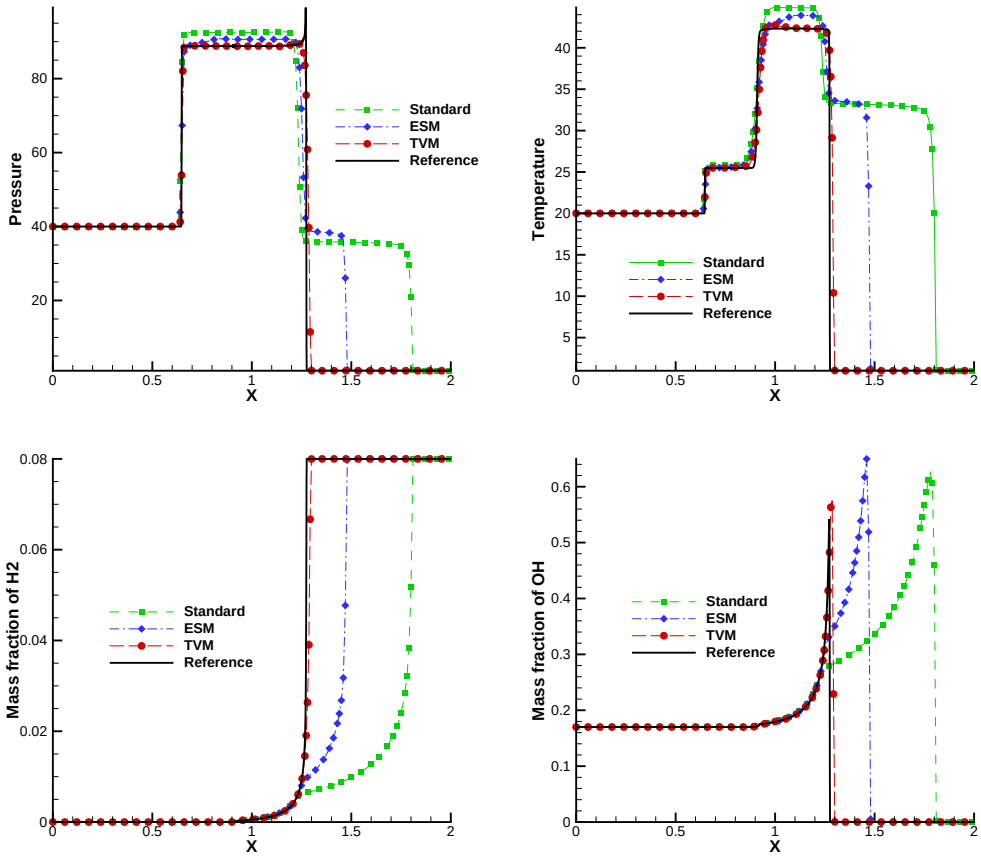


Figure 15: Computed results for multi-reaction case at $t=0.06$. All methods with $N=300$ except for reference solution with $N=4000$ by standard dissipative method.

# Acknowledgments

The authors would like to thank the Center for High Performance Computing of SJTU for providing the super computer $\pi$ to support this research. This work is supported by the National Natural Science Foundation of China (NSFC-91441205 and NSFC-91330203) and National Science Foundation for Young Scientists of China (Grant No. 51606120). Furthermore, Haiyan Lin and Chunhui Tang are appreciated in checking the revised manuscript.

### References

[1] P. Colella, A. Majda and V. Roytburd, Theoretical and numerical structure for reacting shock waves, SIAM J. Sci. Stat. Comput., 7(4) (1986), 1059–1080.

[2] D. Griffiths, A. Stuart and H. C. Yee, Numerical wave propagation in an advection equation with a nonlinear source term, SIAM J. Numer. Anal., 29(5) (1992), 1244–1260.
[3] A. Lafon and H. C. Yee, Dynamical approach study of spurious steady-state numerical solutions of nonlinear differential equations, part iii: the effects of nonlinear source terms in reaction-convection equations, Int. J. Comput. Fluid Dyn., 6(1) (1996), 1–36.
[4] A. Lafon and H. C. Yee, Dynamical approach study of spurious steady-state numerical solutions of nonlinear differential equations part IV: stability vs. methods of discretizing nonlinear source terms in reaction-convection equations, Int. J. Comput. Fluid Dyn., 6(2) (1996), 89–123.
[5] R. J. LeVeque an d H. C. Yee, A study of numerical methods for hyperbolic conservation laws with stiff source terms, J. Comput. Phys., 86(1) (1990), 187–210.
[6] H. C. Yee, D. V. Kotov, W. Wang and C.-W. Shu, Spurious behavior of shock-capturing methods by the fractional step approach: Problems containing stiff source terms and discontinuities, J. Comput. Phys., 241 (2013), 266–291.
[7] H. C. Yee, D. V. Kotov, W. Wang and C.-W. Shu, Corrigendum to "Spurious behavior of shock-capturing methods by the fractional step approach: Problems containing stiff source terms and discontinuities" [J. Comput. Phys., 241 (2013), 266–291], J. Comput. Phys., 250(1) (2013), 703–712.
[8] B. Zhang and J.-H. Wang, A short note on the counter-intuitive spurious behaviors in stiff reacting flow, J. Comput. Phys., 291 (2015), 52–59.
[9] B. L. Bihari and D. Schwendeman, Multiresolution schemes for the reactive euler equations, J. Comput. Phys., 154(1) (1999), 197–230.
[10] R. Jeltsch and P. Klingenstein, Error estimators for the position of discontinuities in hyperbolic conservation laws with source terms which are solved using operator splitting, Comput. Visual. Sci., 1(4) (1999), 231–249.
[11] R. J. Leveque and K.-M. Shyue, One-dimensional front tracking based on high resolution wave propagation methods, SIAM J. Sci. Comput., 16(2) (1995), 348–377.
[12] D. Nguyen, F. Gibou and R. Fedkiw, A fully conservative ghost fluid method and stiff detonation waves, in: 12th Int. Detonation Symposium, San Diego, CA, 2002.
[13] Y. Sun and B. Engquist, Heterogeneous multiscale methods for interface tracking of combustion fronts, Multiscale Modeling & Simulation, 5(2) (2006), 532–563.
[14] A. J. Chorin, Random choice solution of hyperbolic systems, J. Comput. Phys., 22(4) (1976), 517–533.
[15] A. J. Chorin, Random choice methods with applications to reacting gas flow, J. Comput. Phys., 25(3) (1977), 253–272.
[16] A. Majda and V. Roytburd, Numerical study of the mechanisms for initiation of reacting shock waves, SIAM J. Sci. Stat. Comput., 11(5) (1990), 950–974.
[17] C. Helzel, R. J. Leveque and G. Warnecke, A modified fractional step method for the accurate approximation of detonation waves, SIAM J. Sci. Comput., 22(4) (2000), 1489–1510.
[18] W. Bao and S. Jin, The random projection method for hyperbolic conservation laws with stiff reaction terms, J. Comput. Phys., 163(1) (2000), 216–248.
[19] W. Bao and S. Jin, The random projection method for stiff detonation capturing, SIAM J. Sci. Comput., 23(3) (2001), 1000–1026.
[20] W. Bao and S. Jin, The random projection method for stiff multispecies detonation capturing, J. Comput. Phys., 178(1) (2002), 37–57.
[21] L. Tosatto and L. Vigevano, Numerical solution of under-resolved detonations, J. Comput. Phys., 227(4) (2008), 2317–2343.

[22] W. Wang, C.-W. Shu, H. C. Yee and B. Sjögreen, High order finite difference methods with subcell resolution for advection equations with stiff source terms, J. Comput. Phys., 231(1) (2012), 190–214.
[23] W. Wang, C.-W. Shu, H. C. Yee, D. V. Kotov and B. Sjögreen, High order finite difference methods with subcell resolution for stiff multispecies discontinuity capturing, Commun. Comput. Phys., 17(02) (2015), 317–336.
[24] B. Zhang, H. Liu, F. Chen and J. H. Wang, The equilibrium state method for hyperbolic conservation laws with stiff reaction terms, J. Comput. Phys., 263 (2014), 151–176.
[25] M. Ben-Artzi, The generalized riemann problem for reactive flows, J. Comput. Phys., 81(1) (1989), 70–101.
[26] A. Berkenbosch, E. Kaasschieter and R. Klein, Detonation capturing for stiff combustion chemistry, Combustion Theory Modelling, 2(3) (1998), 313–348.
[27] A. Bourlioux, A. J. Majda and V. Roytburd, Theoretical and numerical structure for unstable one-dimensional detonations, SIAM J. Appl. Math., 51(2) (1991), 303–343.
[28] A. Hidalgo and M. Dumbser, Ader schemes for nonlinear systems of stiff advection–diffusion–reaction equations, J. Sci. Comput., 48(1-3) (2011), 173–189.
[29] F. Miniati and P. Colella, A modified higher order godunovs scheme for stiff source conservative hydrodynamics, J. Comput. Phys., 224(2) (2007), 519–538.
[30] R. B. Pember, Numerical methods for hyperbolic conservation laws with stiff relaxation I, spurious solutions, SIAM J. Appl. Math., 53(5) (1993), 1293–1330.
[31] V. T. Ton, Improved shock-capturing methods for multicomponent and reacting flows, J. Comput. Phys., 128(1) (1996), 237–253.
[32] J. D. Anderson, Hypersonic and high temperature gas dynamics, AIAA, 2000.
[33] G. Strang, On the construction and comparison of difference schemes, SIAM J. Numer. Anal., 5(3) (1968), 506–517.
[34] A. Kurganov and E. Tadmor, New high-resolution central schemes for nonlinear conservation laws and convection–diffusion equations, J. Comput. Phys., 160(1) (2000), 241–282.
[35] M.-S. Liou and C. J. Steffen, A new flux splitting scheme, J. Comput. Phys., 107(1) (1993), 23–39.
[36] M.-S. Liou, A sequel to ausm: Ausm+, J. Comput. Phys., 129(2) (1996), 364–382.
[37] J. C. Butcher, The Numerical Analysis of Ordinary Differential Equations: Runge-Kutta and General Linear Methods, Wiley-Interscience, 1987.
[38] D. V. Kotov, H. C. Yee, M. Panesi, D. K. Prabhu an d A. A. Wray, Computational challenges for simulations related to the NASA electric arc shock tube (EAST) experiments, J. Comput. Phys., 269(1) (2014), 215–233.